Au/ZrO_2 catalysts for low-temperature water gas shift reaction: Influence of particle sizes

Juan Li, Na Ta, Wei Song, Ensheng Zhan, Wenjie Shen*

State Key Laboratory of Catalysis, Dalian Institute of Chemical Physics, Chinese Academy of Sciences, Dalian 116023, China

* Corresponding author: Wenjie Shen
Tel: +86-411-84379085; Fax: +86-411-84694447
E-mail: shen98@dicp.ac.cn

Abstract

The size effects of Au and ZrO_2 particles on the structural property and the catalytic performance of Au/ZrO_2 catalysts for the water gas shift reaction were extensively investigated. It was found that the Au-ZrO_2 contact boundaries played essential roles in determining the catalytic reactivity. By keeping the size of Au particle to be ~3 nm, the increase in the particle size of ZrO_2 from ~7 nm to ~55 nm caused significant decrease in the reaction rate. When the particle size of ZrO_2 was fixed at ~20 nm, the conversion of CO decreased greatly with increasing the size of gold particle from 2.9 to 6.2 nm. IR spectroscopy and kinetic study revealed that the water gas shift reaction occurred at the Au-ZrO_2 contact boundaries, where CO is adsorbed on the Au species and H_2O is activated on the surface of ZrO_2 through the formation of formate species, acting as key reaction intermediates.

Keywords: Au/ZrO_2; Particle size; Contact boundary; Water gas shift; Low-temperature.

1 Introduction

Low-temperature water gas shift (WGS) reaction has recently attracted renewed attention because of its application in hydrogen production for fueling proton exchange membrane fuel cells. The reformed fuel generated by reforming of hydrocarbons and/or alcohols usually contains 1-10% CO, which needs to be removed by the WGS reaction for preventing the Pt electrode from being poisoned by CO adsorption (1-3). Gold nanoparticles supported by CeO_2 and ZrO_2 have been proved to be effective for low-temperature WGS in this specific application. The high activity of the Au catalyst relies mainly on the metal-support interaction which strongly depends on the size of Au particle and the nature of the support (4-11).

Since the early report by Fu *et al* (4) that Au/CeO_2 catalyst is very active and stable for the WGS reaction, there have been substantial interests in the origin of the exceptional catalytic property (12-16) and the underlying reaction mechanism (11,12,17-20). However, the intrinsic active site as well as the reaction pathway for the WGS on Au/CeO_2 catalysts is still controversial. Fu *et al* (13,14) revealed that the WGS activities are not altered even when 90% of the gold is removed from the surface of CeO_2 by cyanide leaching, providing clear evidence that metallic gold nanoparticle does not participate in the WGS reaction, but rather that the active site is the cationic gold species which is strongly associated with surface cerium-oxygen groups. It was proposed that the diffusion of Au ions into ceria lattice takes place during the preparation process, leading to a stable presence of cationic gold clusters. In contrast, Kim and Thompson (15) and Karpenko et al (16) observed a significant reduction in the WGS activity on leached Au/CeO_2 catalysts and thus concluded that nanocrystalline gold represents the active site for the WGS reaction, instead of the cationic gold clusters. However, it should be noted that the condition of leaching was not the same as the procedure of Fu *et al* (13, 14), but the leaching was applied to an unconditioned raw catalyst, instead of the calcined sample. Probably, the active gold is removed by the cyanide solution and the activity of the leached sample is expected to be lower. Very recently, *in situ* X-ray absorption near-edge structure measurement and density function theory calculation (21, 22) have confirmed that only the smaller metallic Au nanoparticles (< 3 nm) are present under the WGS reaction conditions, whereas the cationic gold species is unstable. The high stability was attributed to the strong resistance to the sintering of the small gold clusters in intimate contact with ceria. Accordingly, the reaction was proposed to proceed at the Au-ceria contact boundaries, where CO is adsorbed on the Au particle and H_2O is activated on the surface of CeO_2 (5, 17). In addition to the size and the chemical state of Au particle, the size of ceria is also of decisive importance and a strong shape/crystal plane effect of CeO_2 on the WGS activity has been recently reported (4, 23, 24). Gold supported on ceria nanorods enclosed

by {110} and {100} planes are more active for the WGS reaction than that on ceria nanocubes ({100}) and nanopolyhedra ({100} and {111}), because oxygen vacancies, which are indispensable for stabilizing very fine gold clusters, are easier to form on the CeO_2 {110} planes.

Au/ZrO_2 catalysts are also sufficiently active for the WGS reaction at low temperatures (6-8). The size of gold particle is of prime importance, and smaller Au nanoparticles containing a larger amount of active sites (edge, corner or step) in close contact with zirconia usually give quite high WGS activity (6). Meanwhile, the surface property and the crystalline structure of zirconia also influence the catalytic performance significantly (7, 8, 25). Au nanoparticles supported by well crystallized zirconia exhibit higher WGS activity than that on amorphous zirconia (7). Au nanoparticles on monoclinic zirconia could show much better WGS performance than that on tetragonal zirconia because the surface of monoclinic zirconia has more hydroxyl groups favoring to interact with the adsorbed CO on Au particle (8). It is generally agreed that the WGS activity of Au/ZrO_2 catalyst depends strongly on the size of Au particle and the surface property of ZrO_2 support, but the nature of the $Au\text{-}ZrO_2$ interaction as well as the dominant mechanism of the WGS reaction is still unclear.

In this work, we studied the effect of $Au\text{-}ZrO_2$ contact boundaries on the catalytic performance for the WGS reaction by properly tuning the sizes of gold and zirconia particles. Control of the size of ZrO_2 particle was achieved by calcination of the zirconium hydroxide precursor at 450-850°C. Similar loading and particle size of Au on these supports were then obtained by a deposition-precipitation method. The size of Au particle was further adjusted by calcining an Au/ZrO2 catalyst at 250-550°C. The structural properties derived mainly from X-ray power diffraction (XRD) patterns and high-resolution transmission electron microscopy (HRTEM) observations were correlated with the catalytic performance for the WGS reaction.

2 Experimental

2.1 Catalyst preparation

The monoclinic zirconia was prepared by a reflux method described by Jung and Bell (26). 80 g of $ZrOCl_2{\cdot}8H_2O$ was dissolved in 500 ml of deionized H_2O, and the solution was then refluxed at 100°C for 240 h. After the mixture was cooled to room temperature, the pH was slowly adjusted from 1.0 to 10.0 with concentrated ammonia (15 M) aqueous solution to agglomerate the fine particles for facilitating the filtration. The precipitate was dried at 110°C overnight and finally calcined at 450-850°C in air for 4 h. The solid obtained was nominated as ZrO_2-T, where T refers to the temperature of calcination.

The Au/ZrO_2 catalysts with an Au nominal loading of 1.5 wt.% were prepared by a deposition-precipitation method. 3 g of ZrO_2-T powders were dispersed into 300 ml of aqueous solution containing $HAuCl_4$ ($7.6x10^{-4}$ M) and urea (0.5 M). The mixture was heated to 80°C with stirring and kept at this temperature for 4 h with a final pH value of 8.0. After filtration and being washed with hot deionized water, the precipitate was dried at room temperature for 24h and then calcined at 250°C in air flow for 2h. The catalysts obtained were labeled as Au/ZrO_2-T. The Au/ZrO_2-550 catalyst was further calcined at 350, 450 and 550°C in air flow for 2h and labeled as t-Au/ZrO_2, where t denotes the temperature of calcination.

For comparison, the Au/ZrO_2-450 catalyst was treated in an aqueous solution of 0.04 M NaCN for 1h at room temperature for leaching the gold particles, following the procedure of Fu *et al* (13). The resulting solid was washed thoroughly with deionized water, dried at room temperature for 24 h and finally calcined at 250°C in air flow for 2h.

2.2 Catalyst characterization

The actual loading of gold was measured by inductively coupled plasma atomic emission spectroscopy (ICP-AES) on a Plasma-Spec-I spectrometer. Prior to analysis, 100 mg sample was dissolved in 5 ml of aqua regia at 80°C, and the solution was diluted to 25 ml with deionized water.

XRD patterns were recorded using a D/Max-2500/PC powder diffractometer (Rigaku, Japan) with a Cu Ka radiation source operating at 40 kV and 100 mA. The average crystalline size of ZrO_2 was calculated by the Scherrer equation using the (ĩıı) diffraction ($2\theta = 28.2°$).

HRTEM images were taken with a Tecnai G^2 F30 S-Twin microscope (FEI) operating at 300 kV. The sample powders were ultrasonically dispersed in anhydrous ethanol, and a drop of the suspension was deposited on a carbon film supported copper grid, and then dried in air.

N_2 adsorption-desorption isotherms were recorded at −196°C on a Micrometrics ASAP 2000 instrument. Before the measurements, the samples were degassed at 250°C for 5h. The specific surface area was calculated by a multipoint Braunauer-Emmett-Teller (BET) analysis of the nitrogen adsorption isotherm.

X-ray photoelectron spectroscopy (XPS) was recorded with an ESCALAB MK-II spectrometer (VG Scientific Ltd., UK) using Al Kα radiation (λ = 1486.6 eV) operating at an accelerating voltage of 10 kV. The powder samples were pressed into a thin disc and mounted on a sample rod placed in the analysis chamber, where the spectra of C 1s, O 1s, Zr 3d and Au 4f levels were recorded. The charge effect was corrected by adjusting the binding energy of C 1s to 284.6 eV.

Fourier transform infrared (FTIR) spectra were collected over a Biorad Vector 22 spectrometer (Bruker) with a resolution of 4 cm^{-1}, using 32 scans per spectrum in the region of 4000-1000 cm^{-1}. 50 mg of Au/ZrO_2 samples were pressed into a self-supporting pellet and introduced to a cell allowing thermal treatments under controlled atmospheres. The pellet was treated with air flow (40 ml/min) at 250°C for

30 min to remove the adsorbed H_2O and carbonates. After cooling to the measurement temperature with He flow, FTIR spectra were recorded by exposing the sample to a 1%CO/He or 1%CO/3%H_2O/He mixture (40 ml/min). The reference spectrum of the Au/ZrO_2 wafer in He taken at the measurement temperature was subtracted from each spectrum.

Temperature-programmed desorption (TPD) of CO was done in a micro-reactor equipped with a quadrupole mass spectrometer (Omnistar, Balzers). 50 mg of Au/ZrO_2 sample was heated to 250°C with air flow (40 ml/min) and held for 30 min to remove the adsorbed carbonates and hydrates. After cooling to room temperature in He, adsorption of CO was performed by passing a 1% CO/He mixture (40 ml/min) through the sample for 30 min. The sample was then heated to 250°C at a rate of 10°C/min with He flow (40 ml/min). The effluent from the reactor was monitored by the mass spectrometer.

Pulse experiments were performed using the same equipment as TPD measurement. 50 mg of catalyst was pretreated at 250°C in 20% O_2/He flow (40 ml/min) for 30 min. The sample was then purged with He for 30 min at 200°C, and CO or H_2O was pulsed using He (40 ml/min) as carrier gas. Each pulse contained 0.4 ml of pure CO or 1.0 µl of H_2O injected through a microsyringe. The effluent from the reactor was detected by the mass spectrometer.

2.3 Catalytic evaluation

The WGS reaction was conducted in a continuous-flow fixed-bed reactor under atmospheric pressure at 200°C. 100 mg of samples (40-60 mesh) were placed between two layers of quartz wool inside the quartz tube reactor (d = 6 mm). Water was supplied by flowing He over a glass bubbler containing distilled water kept at 51°C. The H_2O/He stream was then mixed with a CO/He mixture coming from a mass flow controller. The feed gas contained 3 vol% CO and 9 vol% H_2O balanced with He, and the typical gas hourly space velocity (GHSV) was 40,000 ml g^{-1} h^{-1}. The Effluent from the reactor was analyzed by an on-line gas chromatograph equipped with a thermal conductivity detector and a flame ionization detector.

Kinetic study was carried out with the same apparatus in the temperature range of 130-170°C. The CO conversion was kept below 15% by adjusting the space velocity in the range 33,500 -100,000 ml g^{-1} h^{-1}. The specific reaction rate was calculated on the basis of the number of Au atoms exposed on the surface, which was estimated from the mean diameter of Au particles and the actual loadings of gold. The shape of Au particles was assumed to be nearly spherical (27).

3 Results and discussion

3.1 Structural characterization

Figure 1 shows the XRD patterns of the zirconium oxides. All the samples exhibited characteristic diffraction peaks of pure

Figure 1

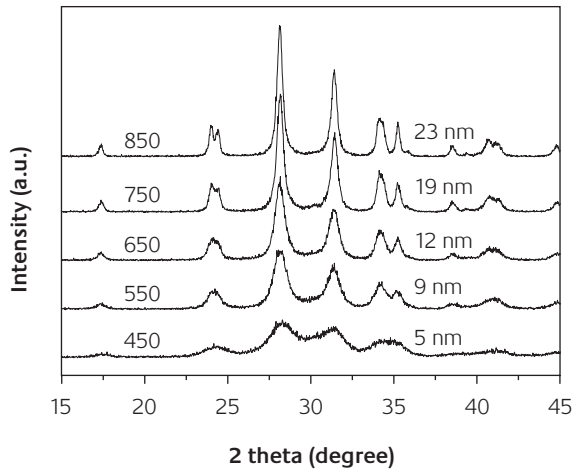

XRD patterns of the zirconium oxides

monoclinic phase at 2θ = 28.2° and 31.3° (JCPDS 37-1484). With increasing the temperature of calcination, the diffraction peaks became sharp and intense, indicating the growth of ZrO_2 crystallite. The crystalline size of ZrO_2 was 5 nm for the ZrO_2-450 sample but it increased rapidly to 23 nm for the ZrO_2-850 sample. Accordingly, the surface area of zirconia decreased from 136 m^2/g to only 16 m^2/g.

Table 1 summarizes the structural properties of the Au/ZrO_2 catalysts. All the samples had similar gold loading of ~1.35 wt.%, and the deposition of gold had little effect on the surface area of zirconia. The XRD patterns of the Au/ZrO_2 catalysts were very similar to those of the corresponding ZrO_2 supports. There were no distinct diffraction peaks of gold, indicating that the gold particles are highly dispersed on ZrO_2 and are too small to be detected.

Figure 2 shows the HRTEM images of the Au/ZrO_2-T catalysts. The ZrO_2 particles apparently agglomerated into larger ones with increasing the temperature of calcination. The Au/ZrO_2-450 sample contained discrete ZrO_2 particles with the size of 5-10 nm; the size of ZrO_2 particles was 10-30 nm in the Au/ZrO_2-550 sample, and then it significantly increased to 30-100 nm for the Au/ZrO_2-850 sample. For the Au particles, they were hardly observed in the Au-ZrO_2-450 catalyst, probably due to the formation of nanocomposite (25). Only a gold particle (2.7 nm) with a lattice spacing of 0.245 nm was occasionally seen. In the remaining samples, Au particles with a hemispherical shape on the ZrO_2 supports were readily discerned. The size of Au particles distributed in 1-7 nm with almost the same average value of ~3 nm, regardless of the size of ZrO_2 particles. This phenomenon is similar to the previous report by Zhang et al (25) who have found that the gold particles have an average size of 4-5 nm when the surface area of ZrO_2 support is in the range 20-162 m^2/g. It seems true that the size of gold particles is

Table 1

Structural Properties and catalytic activities of the Au/ZrO_2 catalysts for the WGS reaction

Sample	S_{BET} (m^2 g^{-1})	Au loading (wt.%)	D_{Au} [a] (nm)	D_{ZrO_2} [a] (nm)	CO_2 desorbed [b] (μmol g^{-1})	CO conv. (%)	Ea (kJ mol^{-1})	Reaction rate[c] (μmol g^{-1} s^{-1})
Au/ZrO_2-450	128	1.32	<2.7	7	93	62	35	3.0
Au/ZrO_2-550	47	1.35	2.9	20	61	57	34	3.0
Au/ZrO_2-650	32	1.33	3.1	30	26	48	33	2.1
Au/ZrO_2-750	21	1.36	2.9	40	17	32	34	1.3
Au/ZrO_2-850	19	1.39	3.0	55	4	12	35	0.8
250-Au/ZrO_2	47	1.35	2.9	20	61	57	34	3.0
350-Au/ZrO_2	47	1.35	3.6	20	62	35	41	1.8
450-Au/ZrO_2	47	1.35	4.2	20	53	18	45	1.0
550-Au/ZrO_2	46	1.35	6.2	20	55	8	47	0.5

[a] *Average particle sizes determined by HRTEM observation. 200 particles were counted for Au particles*

[b] *CO_2 desorbed estimated from CO-TPD profiles*

[c] *Reaction rate of CO measured at 150°C with CO conversion less than 15%*

independent of the size of ZrO_2 particles. Therefore, it becomes possible to elaborate the effect of ZrO_2 particle size on Au-ZrO_2 interaction by keeping constant gold particle size. The Au/ZrO_2-450 sample consists of Au-ZrO_2 nanocomposite mainly due to the size comparability of Au (~2.7 nm) and ZrO_2 (~7 nm) particles, possessing a large amount of Au-ZrO_2 contact boundaries. For the Au/ZrO_2-550 and the Au/ZrO_2-650 samples, the size of ZrO_2 particles is 20-30 nm and a single Au particle (~3 nm) could contact with multiple ZrO_2 particles. For the Au/ZrO_2-750 and the Au/ZrO_2-850 samples with very large ZrO_2 particles of 30-100 nm, however, a single particle of ZrO_2 alone is able to support a number of Au particles and the chance for a single Au particle to make contact with more than one ZrO_2 particle is very rare. That is, the increase in the average size of zirconia particle from ~7 to ~55 nm decreases dramatically the Au-ZrO_2 contact boundaries.

Figure 3 shows the HRTEM images of the t-Au/ZrO_2 catalysts, where the average size of zirconia particle was constant to be ~20 nm. It is obvious that the size of gold particle increased significantly with increasing the temperature of calcination. The size of Au particles was only 2.9 nm after calcination at 250°C and it then increased to 3.6-4.2 nm at 350-450°C, and finally up to 6.2 nm at 550°C. The size distribution of Au particles also became broader with increasing the temperature of calcination. The 250-Au/ZrO_2 sample showed relatively narrow size distribution of 1-7 nm with a maximum at 2-3 nm, and quite a number of particles were below 2 nm. The 350-Au/ZrO_2 and the 450-Au/ZrO_2 samples had size distribution in the range 1-8 nm, with a maximum at 2-3 nm and 3-4 nm, respectively. But the 550-Au/ZrO_2 sample showed a wide size distribution of 2-11 nm with a maximum at 4-5 nm. The fraction of particles of 1-2 nm decreased apparently with increasing the temperature of calcination, suggesting that small Au particles aggregated into large ones during the calcination process.

Figure 4 shows the XP spectra of Au 4f in the t-Au/ZrO_2 catalysts. For all the samples, the binding energies of Au $4f_{7/2}$ and Au $4f_{5/2}$ were 83.6 and 87.3 eV, respectively, characteristics of Au^0 species (28). Since the gold precursor is easy to decompose into Au^0 in air (29), calcination at above 250°C is usually sufficient enough to produce metallic gold particles. Based on EXAFS measurements, Zanella et al (30) also found that the Au/TiO_2 samples contained only metallic Au^0 species even at a calcination temperature of 200°C. Therefore, it is reasonable that the gold particles in the Au/ZrO_2 catalysts present as Au^0.

3.2 FTIR

Figure 5 shows the FTIR spectra of hydroxyl groups in the Au/ZrO_2 catalysts recorded at 200°C. All the samples contained two types of hydroxyl groups with bands at 3743 and 3687 cm^{-1}. The former represents the terminal OH groups and the latter corresponds to the bi- or tri-bridging OH groups (31,32). For the Au/ZrO_2-T catalysts, as shown in Figure 5A, the intensities of the two bands decreased significantly with increasing the size of ZrO_2 particle, indicating that small ZrO_2 particle has relatively higher concentration of surface hydroxyl groups. However, the intensities of these hydroxyl groups in the t-Au/ZrO_2 catalysts having similar ZrO_2 particle size of ~20 nm were essentially the same (Figure 5B), evidencing that the thermal treatment at 250-550°C for producing Au particles does not affect the amount of OH groups on the surface of the ZrO_2 support.

Figure 2

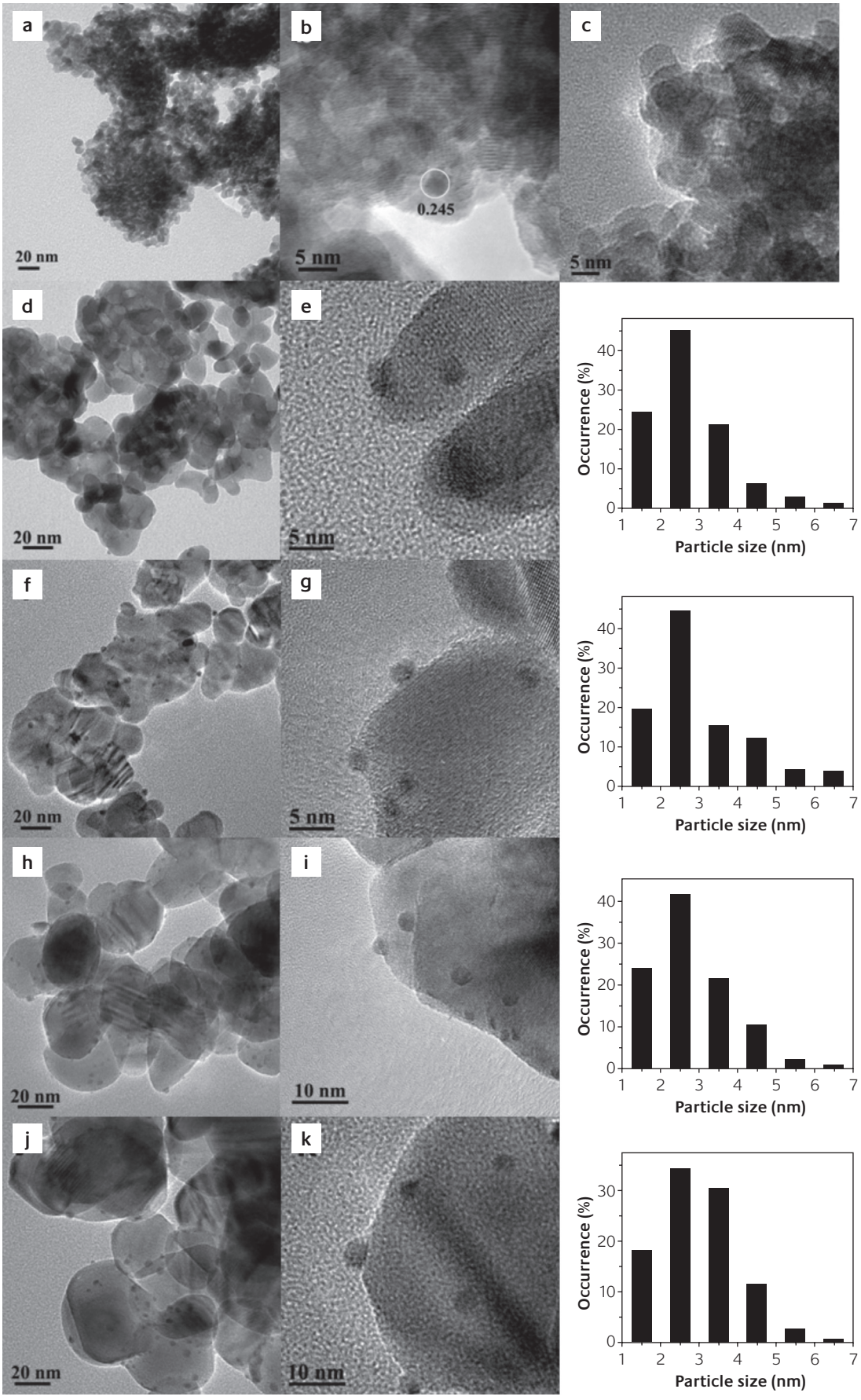

TEM images of the Au/ZrO_2-T catalysts and size distribution of Au particles where T = 450 (a-c), 550 (d, e), 650 (f, g), 750 (h, i) and 850 (j, k)

Figure 3

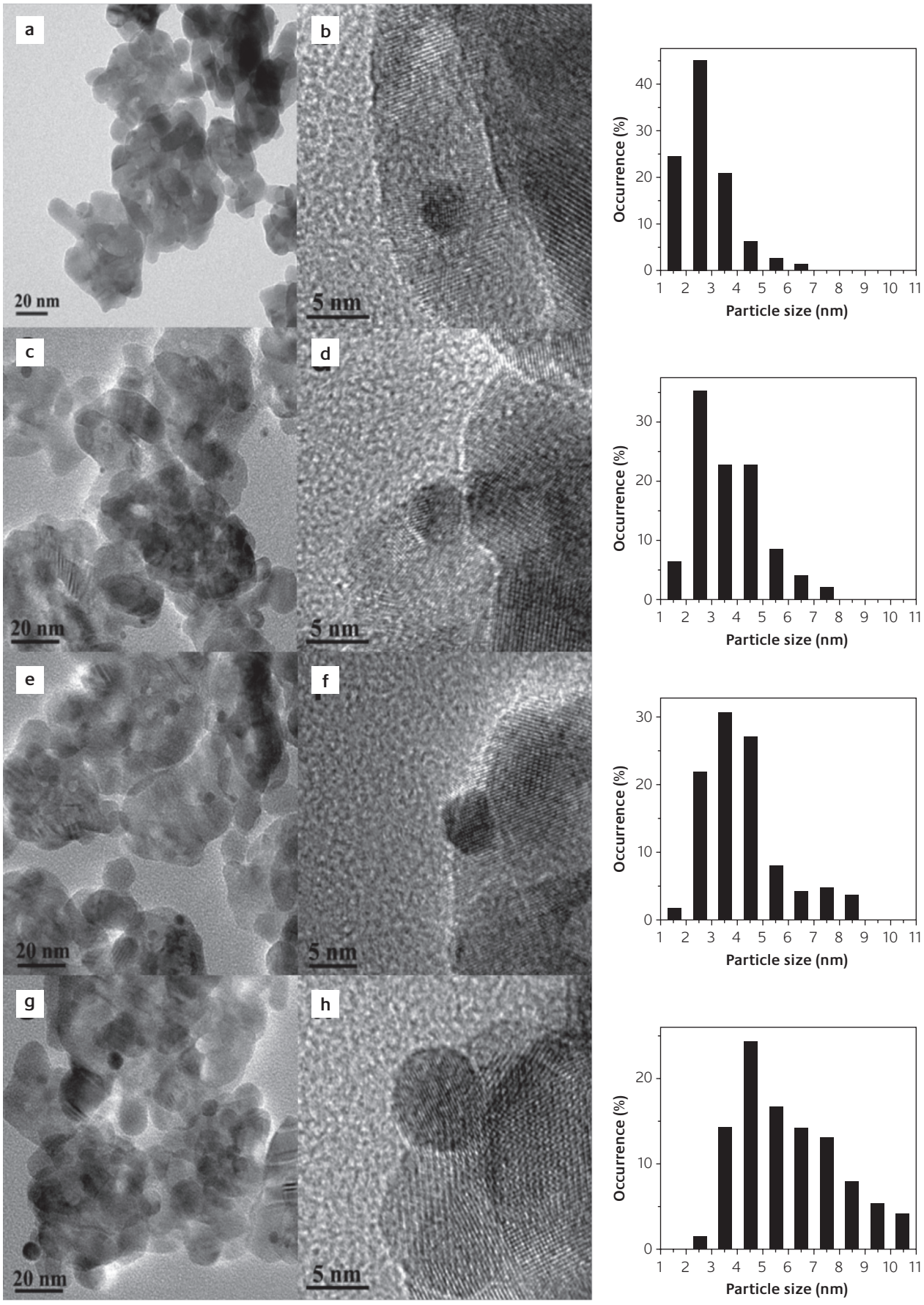

TEM images of the t-Au/ZrO_2 catalysts and size distribution of Au particles where t = 250 (a, b), 350 (c, d), 450 (e, f) and 550 (g, h)

Figure 4

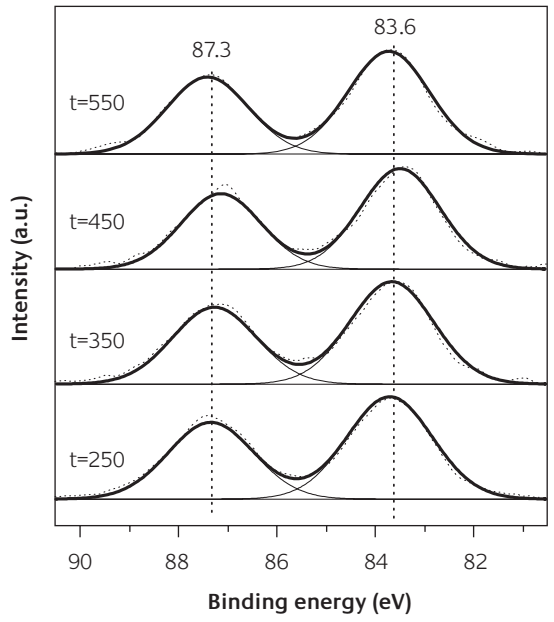

XP spectra of Au 4f in the t-Au/ZrO_2 catalysts

Figure 5

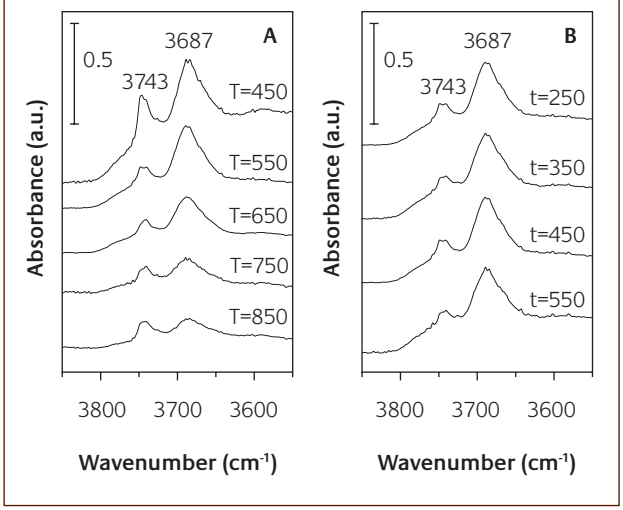

FTIR spectra of hydroxyl groups in the Au/ZrO_2-T (A) and the t-Au/ZrO_2 (B) catalysts

Figure 6

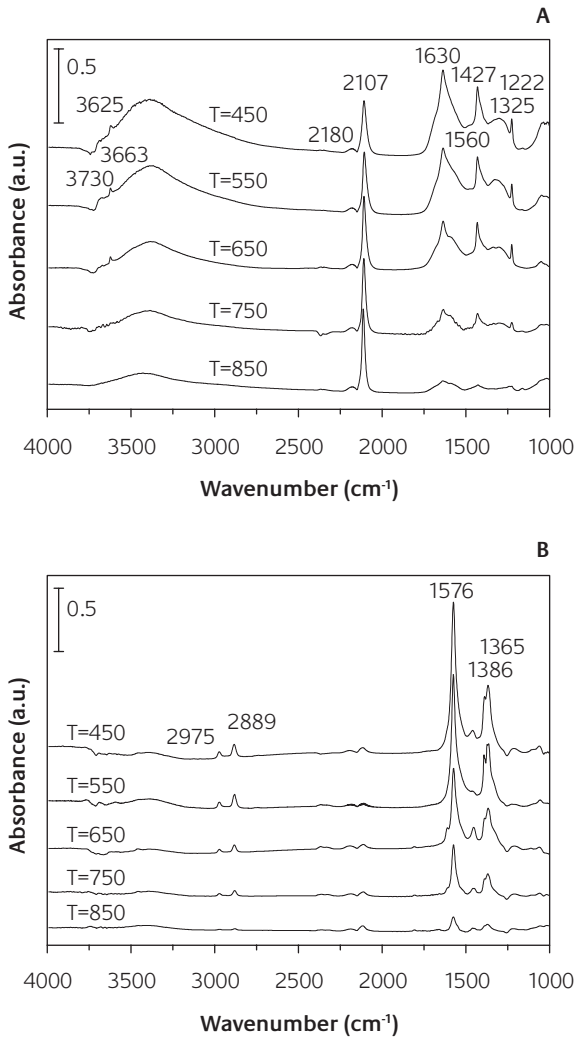

FTIR spectra of CO adsorption on the Au/ZrO_2-T catalysts at 25°C (A) and 200°C (B)

Figure 6 shows the FTIR spectra of CO adsorption on the Au/ZrO_2-T catalysts with similar Au particle size but varying ZrO_2 particle size. At 25°C (Figure 6A), a typical band at 2107 cm^{-1} appeared, which is generally assigned to CO adsorbed linearly on Au^0 particle (33,34). The weak band at 2180 cm^{-1} is characteristic for CO adsorption on surface Zr^{4+} site (34). Bicarbonate species with the bands at 1630, 1427 and 1222 cm^{-1} and bidentate carbonate species with the bands at 1560 and 1325 cm^{-1} (33,35) are also observed. The band at 3625 cm^{-1} is likely due to μ-OH vibration in the bicarbonate species. This fact confirms that bicarbonate species are readily formed through the interaction of CO adsorbed on Au^0 with hydroxyl groups on the surface of ZrO_2 at such a low temperature. More importantly, the relative amount of bicarbonate species decreases with increasing the average size of ZrO_2 particle from 7 to 55 nm, further evidencing the abundant presence of hydroxyl groups on the surface of ZrO_2 with smaller particle size.

At 200°C (Figure 6B), the Au^0-CO bonding at 2107 cm^{-1} became very weak and was hardly detected. The bicarbonate species were no longer observed, whereas formate species with bands at 2975, 2889, 1576, 1386 and 1365 cm^{-1} (17,35) were produced. The intensities of these bands decreased with increasing the average size of ZrO_2 particle, indicating that the formation of formate is associated with the size of ZrO_2 particle, and that smaller ZrO_2 particle containing abundant hydroxyl groups favors the efficient reaction of OH groups with CO adsorbed on Au particle because of the increased Au-ZrO_2 contact boundaries.

Figure 7

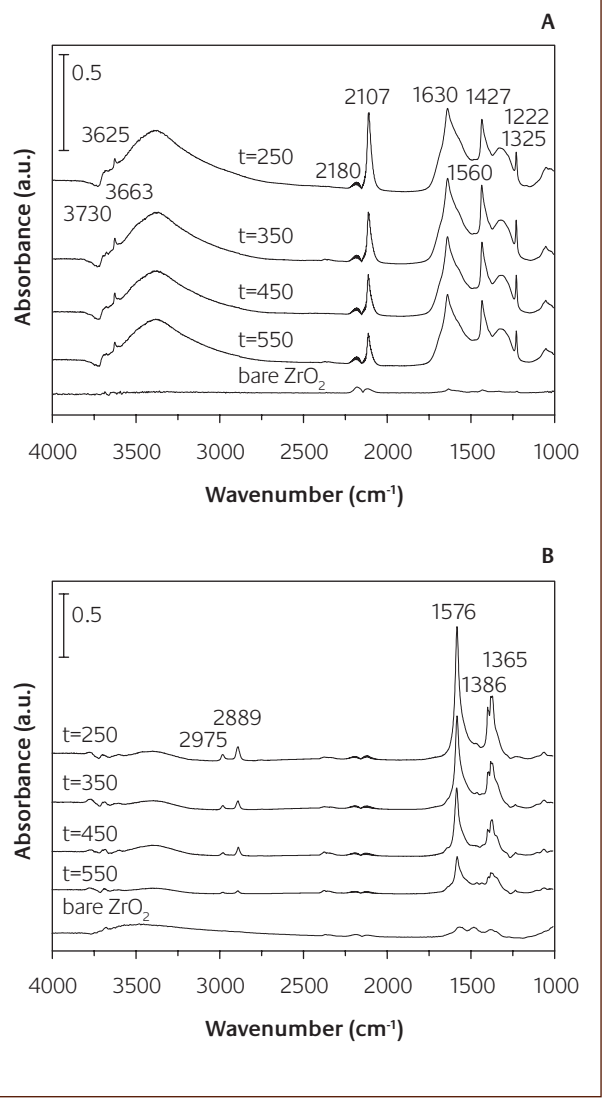

FTIR spectra of CO adsorption on the t-Au/ZrO_2 catalysts at 25°C (A) and 200°C (B)

Figure 7 shows the FTIR spectra of CO adsorption on the t-Au/ZrO_2 catalysts with constant ZrO_2 particle size but different Au particle size. At 25°C, as shown in Figure 7A, the intensity of the band at 2107 cm^{-1} for CO adsorbed linearly on Au^0 decreased gradually with increasing the size of gold particle from 2.9 to 6.2 nm, indicating that the available sites for CO adsorption decreased apparently due to the growth of gold particle. CO adsorption might only occur on the steps, edges and corners associated with smaller Au particles and not on the smooth surface associated with larger ones, as reported by Boccuzzi *et al* (36). The intensities of bicarbonate species in the range 1200-1700 cm^{-1} remained unchanged, suggesting that the formation of these species is not associated with the size of gold particle, but is closely related with the size of ZrO_2 particle. For bare ZrO_2, very weak CO adsorption on surface Zr^{4+} site was observed and only a very small amount of carbonates was detected.

Figure 8

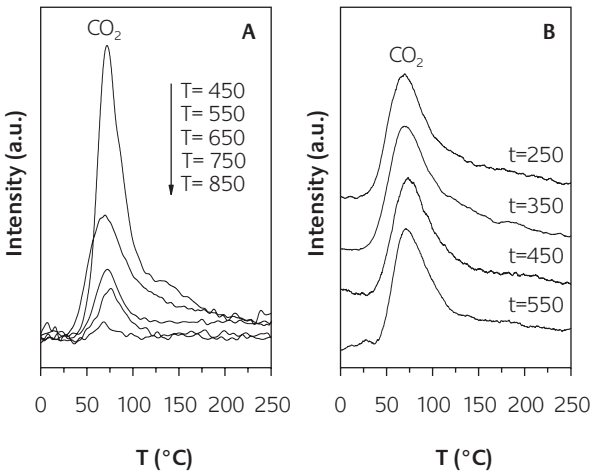

CO-TPD profiles of the Au/ZrO_2-T (A) and the t-Au/ZrO_2 (B) catalysts

At 200°C (Figure 7B), the intensities of formate species on the t-Au/ZrO_2 catalysts decreased greatly with increasing the size of gold particle. However, formate species were hardly observed on bare ZrO_2, clearly indicating that the interaction of between CO and OH groups is very weak in the absence of Au particle. Therefore, it can be proposed that CO is mainly adsorbed on Au particle and then spills over to Au-ZrO_2 contact boundaries, where it further reacts with the OH groups on ZrO_2 to produce formate species. With increasing the size of gold particle, the available sites for CO adsorption and the Au-ZrO_2 contact boundaries decrease simultaneously, and thus the spill over of CO is depressed, leading to less formation of formate species. Therefore, the size of Au particle is crucial not only for the adsorption of CO but also for the surface reaction and small gold particle favors the production of abundant formate species.

3.3 CO-TPD

Figure 8 shows the CO-TPD profiles of the Au/ZrO_2 catalysts. Only desorption of CO_2 at about 80°C was detected due to the decomposition of bicarbonate species, which were readily formed upon CO adsorption at room temperature as confirmed by the FTIR measurements. For the Au/ZrO_2-T catalysts with constant Au particle size but varying ZrO_2 particle size, the amount of CO_2 desorbed decreased with increasing the size of ZrO_2 particle, as shown in Table 1. It is 93 μmol g^{-1} when the average size of ZrO_2 particles is 7 nm and decreases rapidly to 4 μmol g^{-1} for the large ZrO_2 particles with an average size of 55 nm. This fact indicates that relatively higher concentration of OH groups is present on the surface of the catalyst with smaller ZrO_2 particles. For the t-Au/ZrO_2 catalysts with same ZrO_2 particle size but different Au particle size, the amount of CO_2 desorbed was very close (53-62 μmol/g), suggesting that the size of Au particle in the

Figure 9

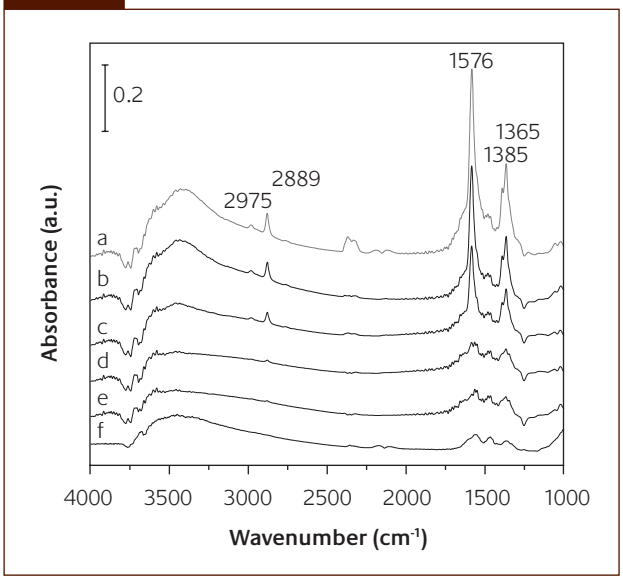

FTIR spectra of the Au/ZrO_2-450 catalyst exposed to 1%CO/3%H_2O/He stream at 200°C for 1 h (a), followed by He purging for 3 min (b), 5 min (c), 8 min (d), 10 min (e) and the bare ZrO_2 support exposing to 1%CO/3%H_2O/He stream for 1 h (f)

range 2.9-6.2 nm does not influence the surface reaction of CO and OH groups to form bicarbonate species at room temperature. For ZrO_2 alone, however, the amount of CO_2 desorbed was nearly negligible when compared with the Au/ZrO_2 catalysts, implying that the role of Au nanoparticle is to provide adsorption site for CO and to promote its surface reaction with OH groups on ZrO_2.

3.4 Reaction mechanism

Figure 9 shows the FTIR spectra of the Au/ZrO_2-450 catalyst recorded during the WGS reaction at 200°C. The buildup of formate on the surface of the catalyst was clearly identified by the characteristic C-H vibration at 2975 and 2889 cm^{-1} and the typical bonds at 1576, 1386 and 1365 cm^{-1} in the COO region (17, 35). These formate species are probably produced by the reaction of CO adsorbed on gold particle with OH groups on the surface of ZrO_2. On the other hand, however, it is hardly to detect the presence of formate species on bare ZrO_2 support under the same reaction conditions. This fact indicates that the Au particle promotes the formation of formate species through CO adsorption and spilling over to the Au-ZrO_2 contact boundaries. When the reaction gas CO/H_2O/He is switched to inert He, the bands associated with formate species gradually reduced their intensities with prolonging the purging time. After 10 min, formate species decomposed completely and only a small quantity of carbonate species retained on the surface.

Figure 10 shows the results of sequential pulses of CO and H_2O under flowing He over the Au/ZrO_2-450 catalyst at 200°C. CO injection resulted in the simultaneous formation of CO_2 and H_2. Since the only source of hydrogen is the surface hydroxyl groups, the formation of CO_2 and H_2 can be described by the following equation:

$$Au{-}CO + OH_{(s)} \rightarrow (COOH)_{(s)} \rightarrow CO_{2(g)} + 1/2H_{2(g)} + Au + *_{(s)}, \quad (1)$$

Where $_{(s)}$ and $*_{(s)}$ denote the surface of ZrO_2 and the surface vacancy on it, respectively. This observation implies that the

Figure 10

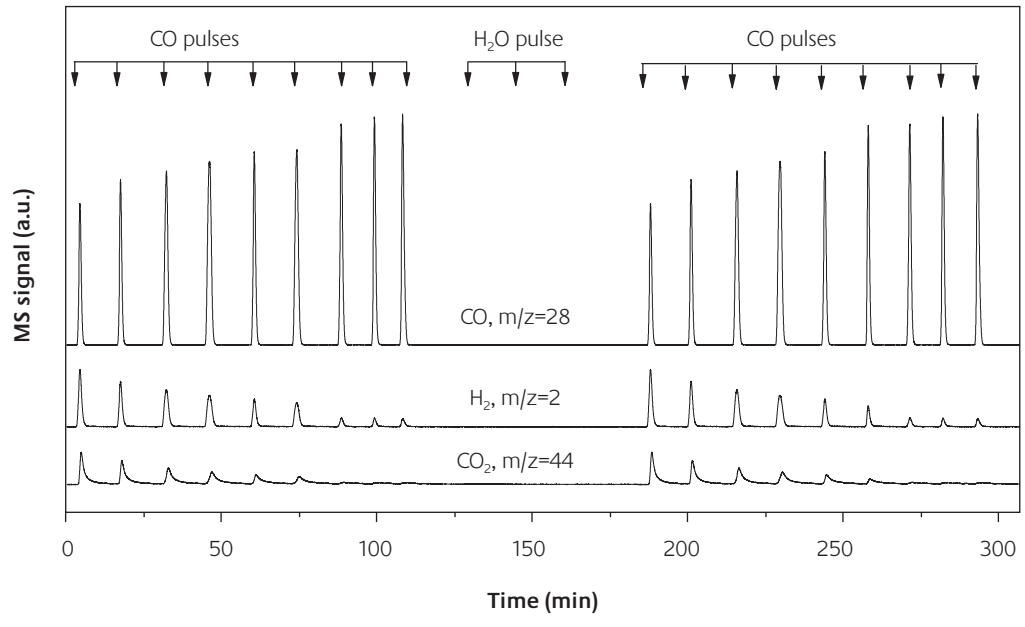

MS signal during CO and H_2O sequential pulse injections over the Au/ZrO_2-450 catalyst under flowing He at 200°C

Figure 11

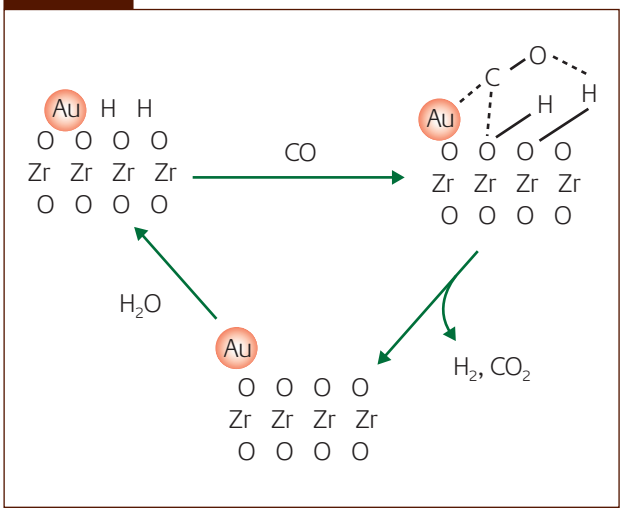

Possible reaction pathway for the WGS reaction on the Au/ZrO_2 catalyst

formate species, once formed, are easy to decompose into CO_2 and H_2. With additional CO pulses, the amount of CO consumed decreased gradually and only traces of CO_2 and H_2 were detected after nine injections, indicating that the surface OH groups are almost completely consumed. Interestingly, H_2O pulses did not produce any gaseous products, but the subsequent CO pulses produced CO_2 and H_2 again. It means that the pulsed H_2O have regenerated the surface OH groups previously removed by CO titration, following the reaction scheme below:

$$*_{(s)} + O_{(s)} + H_2O \rightarrow 2OH_{(s)}. \quad (2)$$

The exact nature of the key intermediates and the dominating mechanism for the WGS reaction over supported gold catalysts are still under debate, even for the most extensively studied Au/CeO_2 catalysts. To date, there is no clear agreement over the prime mechanistic pathway probably due to the choice of metal oxide as support and the variation in reaction conditions. There are two major mechanisms: a redox mechanism based on the reduction of CeO_2 support by CO adsorbed on Au particle to release CO_2 and the subsequent re-oxidation of the partially reduced ceria by H_2O to release H_2 (4,19); and an associative mechanism where CO adsorbed on Au particle reacts with surface OH groups on the support (CeO_2 or ZrO_2) to form formate species which act as the important intermediates involving in the rate-determining step (5,8,17-19). Very recently, Burch (12) has proposed an integrated mechanism for WGS reaction over an Au/CeO_2 catalyst, in which the dominant species changes from a carbonate or carboxylate species to a formate species with increasing the temperature, and eventually at high temperatures to a mechanism that is characteristic of a redox process.

CO/H_2O pulse experiments and *in situ* FTIR spectra on the Au/ZrO_2 catalyst confirm that the dominant reaction pathway under the current experimental conditions might be the formate route in conjunction with the surface regeneration of the ZrO_2 support. As illustrated in Figure 11, CO is initially adsorbed on the gold nanoparticle, and then spills over to the Au–ZrO_2 interface, where it reacts with the surface OH groups on ZrO_2 to produce formate species. CO_2 is formed by abstracting oxygen from the OH groups together with the release of H_2, leaving surface vacancies. H_2O then interacts with the surface of zirconia to regenerate the OH groups. Here, the ZrO_2 support plays an important role in the activation of water for a closure of the catalytic cycle.

3.5 WGS reaction

Figure 12 shows the CO conversions as a function of time-on-stream (TOS) over the Au/ZrO_2-T catalysts. The conversion of CO decreased significantly with increasing the size of ZrO_2 particle. The conversion of CO was 62% for the Au/ZrO_2-450 catalyst with ZrO_2 particle size of ~7 nm, but it decreased rapidly to 12% for the Au/ZrO_2-850 sample with ZrO_2 particle size of ~55 nm. Since the size of gold particle is almost the same in these catalysts, the difference in CO conversion could be attributed to the size effect of ZrO_2 particle. Small ZrO_2 particle not only increases the Au-ZrO_2 contact boundaries acting as the active sites for the WGS reaction (5,8,17), but also modifies the chemical properties of the boundaries due to the presence of a larger number of active hydroxyl groups (37) and oxygen vacancies (38) on the surface. The hydroxyl groups and oxygen vacancies are found to be important in the activation of water and the formation of formate species (8,17,39), which are the key intermediates in the WGS reaction. FTIR and CO-TPD experiments have readily demonstrated that the relatively higher concentration of hydroxyl groups present on the surface of zirconia with smaller particle sizes contributed to a higher concentration of formate species. Therefore, the concentration of formate species gives an important indication of the number of active sites, and consequently, the WGS reaction activity, which are greatly enhanced with reducing the average size of ZrO_2 particle.

Figure 13 shows the reaction rates of the WGS reaction on the Au/ZrO_2-T catalysts under differential conditions. The apparent activation energy (E_a) was ~34 kJ mol^{-1}, as shown in Table 1, which is independent of the size of zirconia particle. This value is comparable to the data previously reported for Au/CeO_2 and Au/TiO_2 catalysts (17,40).The reaction rate of CO was very close between the Au/ZrO_2-450 (ZrO_2, 7 nm) and the Au/ZrO_2-550 (ZrO_2, 20 nm) catalysts, and then it decreased with a further increase in the size of ZrO_2 particle. Interestingly, the reaction rate of CO over the Au/ZrO_2-450 catalyst was three times higher than that over the Au/ZrO_2-850 catalyst. Zhang *et al* (25) reported that the specific reaction rate over the Au/ZrO_2 catalyst with ZrO_2 size of 5-10 nm is six times larger than that with ZrO_2 size of 40-200 nm in CO oxidation. Carrettin *et al* (41) also found that

Figure 12

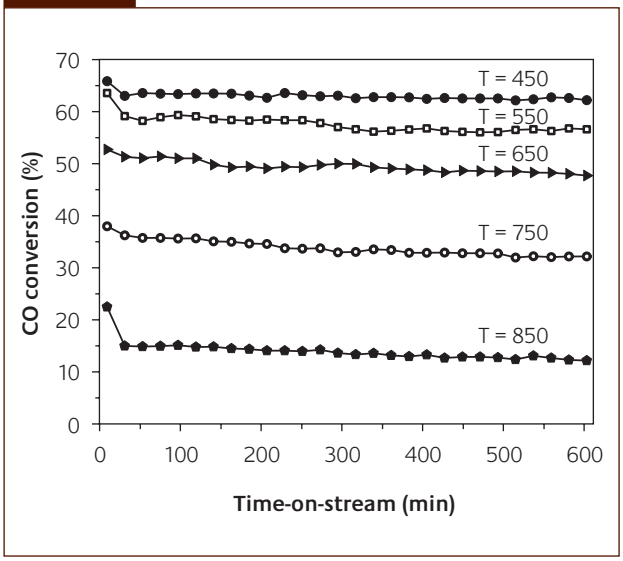

CO conversions over the Au/ZrO_2-T catalysts. Reaction conditions: 200°C; 3%CO/9%H_2O/He; 40,000 ml g^{-1} h^{-1}

Figure 13

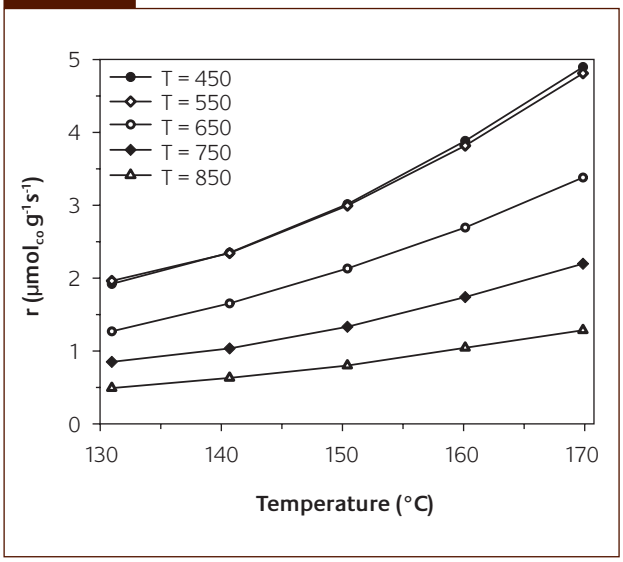

Reaction rates of CO on the Au/ZrO_2-T catalysts. Reaction conditions: 3%CO/9%H_2O/He; 33,500-100,000 ml g^{-1} h^{-1}

nanocrystalline CeO_2 with size of ~4 nm increases the activity of gold for CO oxidation by two orders of magnitude with respect to the conventional CeO_2 particles. Apparently, the reaction rate of CO is affected by the particle size of the oxide support through a strong metal-support interaction. Similar situation could be applied to the current Au-ZrO_2 system for WGS reaction. In addition to increasing surface hydroxyl groups and oxygen vacancies, the decrease in the size of ZrO_2 particle would increase the Au-ZrO_2 contact boundaries. This favors an easier CO migration or spill over from Au clusters or particles to the Au-ZrO_2 interface to produce formate species acting as key reaction intermediates.

Figure 14 shows the CO conversions over the t-Au/ZrO_2 catalysts. The conversion of CO decreased rapidly from 57% to 8% with increasing the size of gold particle from 2.9 to 6.2 nm. Figure 15 shows the reaction rates of CO on the t-Au/ZrO_2 catalysts under differential conditions. The reaction rate of CO decreased dramatically with increasing the size of Au particle from 2.9 to 6.2 nm, particularly below 4 nm, and the difference became more striking with increasing the reaction temperature from 130 to 170°C. The apparent activation energy depended on the size of gold particle strongly, which increased from 34 to 47 kJ mol^{-1} with increasing the size of Au particle from 2.9 to 6.2 nm (Table 1). This phenomenon suggests that the dominating contribution to the activation energy originates from a reaction step associated with Au particle, probably the adsorption and spill over of CO. This observation is in accord with the general understanding that the WGS activity of gold catalyst is very sensitive to the size of gold particle, and the most active catalysts comprise gold primarily in a metallic state but in intimate contact with the support (12). The small Au particle is basically hemispherical with the flat planes strongly attached to the surface of ZrO_2 (Figure 3b), whereas the large Au particle is nearly spherical and simply locates on the surface of ZrO_2 (Figure 3h). In addition, the small Au particle contains a larger proportion of low-coordinated sites (steps, edges and corners) (42,43) and/or Au clusters comprised of Au atoms bound on the zirconia surface, providing more active sites on the Au-ZrO_2 contact boundaries for an efficient adsorption of CO and a rapid surface reaction of CO with OH groups. Therefore, the dramatic difference in the reaction rate of CO due to the variation in the sizes of gold and zirconia particles suggests that the Au-ZrO_2 contact boundary is the most critical factor for the WGS reaction.

Figure 14

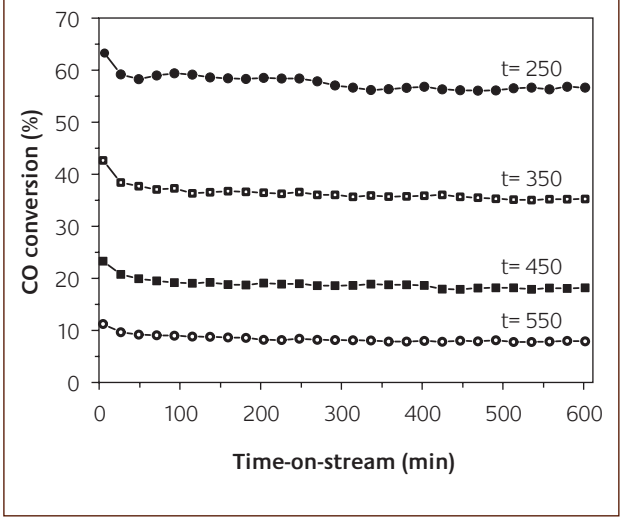

CO conversions over the t-Au/ZrO_2 catalysts. Reaction conditions: 200°C; 3%CO/9%H_2O/He; 40,000 ml g^{-1} h^{-1}

Figure 15

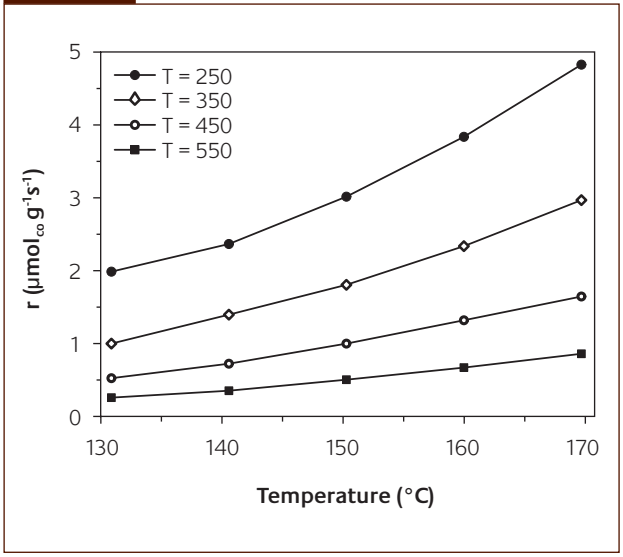

Reaction rates of CO on the t-Au/ZrO_2 catalysts. Reaction conditions: 3%CO/9%H_2O/He; 33,500-100,000 ml g^{-1} h^{-1}

3.6 NaCN leaching

The essential work by Fu *et al* (13,14) has revealed that sodium cyanide can effectively remove the large gold particles and remain the cationic gold clusters locating in the matrix of ceria crystallite acting as the intrinsic active sites for WGS reaction. Zhang *et al* (44) also found that the isolated Au^{3+} ions on zirconia obtained by treating the Au/ZrO_2 catalyst with KCN solution exhibit a much higher activity for selective hydrogenation of 1,3-butadiene than the original catalyst. For comparison, the Au/ZrO_2-450 catalyst with gold loading of 1.35 wt.% was leached with an aqueous solution of 0.04 M NaCN. A majority of gold particles were leached and only trace of gold (0.028 wt.%) retained on the surface of zirconia. This residual gold amount is much less than that in the case of Au/CeO_2 catalyst (13), probably because of the difference in the properties between ceria and zirconia. Ceria is well known to stabilize transitional metal ions in its matrix due to the characteristic cubic fluorite structure and a facile Ce^{4+}/Ce^{3+} redox cycle, generating a lot of oxygen defects, whereas lattice substitution by other ions is difficult for zirconia because of its non-reducible nature. Considering the initial size distribution of gold particle (Figure 2), the remaining gold after leaching should be very small clusters (< 1 nm) probably comprised of Au atoms which are strongly associated with the surface of ZrO_2. The conversion of CO was 62% at 200°C over the parent Au/ZrO_2-450 catalyst, but it was only 12% for the leached sample. This result is very different from the Au/CeO_2 catalyst where the WGS rates for the parent and the leached samples are essentially the same because the cationic gold clusters strongly associated with ceria lattice present the only active sites in WGS reaction (13,14). The dispersion of gold in the parent Au/ZrO_2-450 catalyst is estimated to be 47% based on HRTEM observation (2.7 nm), while a 100% dispersion of gold can be assumed in the leached sample because of the very small clusters. Accordingly, the specific reaction rate of CO for the leached catalyst is about four times greater than that for the parent catalyst, further confirming that very small gold particle is more intrinsically active than the large particle.

It becomes clear that the sizes of Au and ZrO_2 particles greatly affect on the WGS activity. As the size of Au particle is ~3 nm, the WGS activity decreases significantly with increasing the size of ZrO_2 particle from ~7 to ~55 nm as expressed by CO conversion and its reaction rate. On the other hand, when the size of ZrO_2 particle is kept at ~20 nm, the WGS activity decreases remarkably with increasing the size of Au particle from ~2.9 to ~6.2 nm. Both cases reduce the Au-ZrO_2 contact boundaries for the associative surface reaction. Particularly, the Au/ZrO_2-450 catalyst consisting of Au particles with an average size of 2.7 nm and ZrO_2 particles with a mean size of 7 nm possesses the optimal Au-ZrO_2 contact boundaries and thus gives the most promising WGS activity. When the size of Au particle is further decreased to less than 1 nm by cyanide-leaching, however, the overall WGS activity lowers significantly because of the heavy loss in gold amount. But the specific reaction rate on these gold clusters (<1 nm) is much higher than that of the large particles. This fact indicates that both gold nanoparticles (>2 nm) and clusters (<1 nm) jointly participate in the WGS reaction, and the tiny gold clusters are more active than the particles due to the strong interaction with ZrO_2.

4 Conclusions

The activity of Au/ZrO_2 catalysts for low-temperature WGS reaction could be greatly improved by reducing the sizes of zirconia and gold particles, which affected significantly the Au-ZrO_2 contact boundaries where the reaction takes place. For the Au/ZrO_2-T catalysts with similar Au particle size, the increase in the size of ZrO_2 particle decreased the concentrations of surface OH groups as well as the Au-ZrO_2 periphery, leading to a remarkably reduced reaction rate. For the t-Au/ZrO_2 catalysts with constant ZrO_2 particle size, the WGS reactivity decreased rapidly with increasing the size of Au particle because of the reduced available adsorption sites for CO adsorption and Au-ZrO_2 contact boundaries for surface reaction. Variations in the sizes of gold and zirconia particles modify the Au-ZrO_2 contact structure which is the most critical factor for the occurring of WGS reaction. The dominant reaction pathway for the WGS reaction on the current Au/ZrO_2 catalyst is the associative formate route with surface regeneration of the zirconia support.

About the authors

Ms. Juan Li is a PhD candidate at Dalian Institute of Chemical Physics, Chinese Academy of Sciences. Her research topic is gold nanoparticles supported on zirconia and ceria for the water gas shift reaction at low temperatures dating from 2003. Her experience includes design and synthesis of metal and metal oxide nanomaterials, structure analysis and catalytic reaction kinetics.

Dr. Wenjie Shen is a Professor at Dalian Institute of Chemical Physics, Chinese Academy of Sciences. His scientific interests focus on catalytic materials and reaction chemistry, including synthesis of multi-dimensional nanomaterials, size/morphology implications, and catalytic reaction mechanism and kinetics.

References

1 D.L. Trimm and Z.I. Önsan, *Catal. Rev. Sci. Eng.*, 2001, **43**, 31
2 A.N. Fatsikostas, D.I. Kondarides and X.E. Verykios, *Catal. Today*, 2002, **75**, 145
3 C.C. Elam, C.E.G. Padró, G. Sandrock, A. Luzzi, P. Lindblad and E.F. Hagen, *Int. J. Hydrogen Energy*, 2003, **28**, 601
4 Q. Fu, A. Weber and M. Flytzani-Stephanopoulos, *Catal. Lett.* 2001, **77**, 87
5 T. Tabakova, F. Boccuzzi, M. Manzoli, J.W. Sobczak, V. Idakiev and D. Andreeva, *Appl. Catal. A*, 2006, **298**, 127
6 V. Idakiev, T. Tabakova, A. Naydenov, Z.Y. Yuan and B.L. Su, *Appl. Catal. B*, 2005, **63**, 178
7 T. Tabakova, V. Idakiev, D. Andreeva and I. Mitov, *Appl. Catal. A*, 2000, **202**, 91
8 J. Li, J.L. Chen, W. Song, J.L. Liu and W.J. Shen, *Appl. Catal. A*, 2008, **334**, 321
9 A.A. Fonseca, J.M. Fisher, D. Ozkaya, M.D. Shannon and D. Thompsett, *Top. Catal.*, 2007, **44**, 223
10 T. Tabakova, F. Boccuzzi, M. Manzoli, J.W. Sobczak, V. Idakiev and D. Andreeva, *Appl. Catal. B*, 2004, **49**, 73
11 D. Andreeva, *Gold Bull.*, 2002, **35**, 82
12 R. Burch, *Phys. Chem. Chem. Phys.*, 2006, **8**, 5483
13 Q. Fu, H. Saltsburg and M. Flytani-Stephanopoulos, *Science*, 2003, **301**, 935
14 Q. Fu, W. Deng, H. Saltsburg and M. Flytzani-Stephanopoulos, *Appl. Catal. B*, 2005, **56**, 57
15 C.H. Kim and L.T. Thompson, *J. Catal.*, 2006, **244**, 248
16 A. Karpenko, R. Leppelt, V. Plzakb, and R.J. Behma, *J. Catal.*, 2007, **252**, 231
17 R. Leppelt, B. Schumacher, V. Plzak, M. Kinne and R.J. Behm, *J. Catal.*, 2006, **244**, 137
18 G. Jacobs, S. Ricote and B.H. Davis, *Appl. Catal. A*, 2006, **302**, 14
19 D. Andreeva, V. Idakiev, T. Tabakova, L. Ilieva, P. Falaras, A. Bourlinos and A. Travlos, *Catal. Today*, 2002, **72**, 51
20 F.C. Meunier, D. Reida, A. Goguet, S. Shekhtman, C. Hardacre, R. Burcha, W. Deng and M. Flytzani-Stephanopoulos, *J. Catal.* 2007, **247**, 269
21 D. Tibiletti, A. Amieiro-Fonseca, R. Burch, Y. Chen, J.M. Fisher, A. Goguet, C. Hardacre, P. Hu and D. Thompsett, *J. Phys. Chem. B*, 2005, **109**, 22553
22 X. Wang, J.A. Rodriguez, J.C. Hanson, M. Pe' rez and J. Evans, *J. Chem. Phys.*, 2005, **123**, 221101
23 Z.-Y. Yuan, V. Idakiev, A. Vantomme, T. Tabakova, T.-Z. Ren and B.-L. Su, *Catal. Today*, 2008, **131**, 203
24 R. Si and M. Flytzani-Stephanopoulos, *Angew. Chem. Int. Ed.*, 2008, **47**, 2884
25 X. Zhang, H. Wang and B.-Q. Xu, *J. Phys. Chem. B*, 2005, **109**, 9678
26 K.T. Jung and A.T. Bell, *J. Mol. Catal. A*, 2000, **163**, 27
27 G.C. Bond and D.T. Thompson, *Catal. Rev.-Sci. Eng.*, 1999, **41**, 319
28 E.D. Park and J.S. Lee, *J. Catal.*, 1999, **186**, 1
29 G.C. Bond, *Gold Bull.*, 2001, **34**, 117
30 R, Zanella, S, Giorgio, C-H Shin, C.R. Henry and C. Louis, *J. Catal.*, 2004, **222**, 357
31 P.A. Agron, E.L. Fuller and H.F. Holmes, *J. Colloid Interface Sci.*, 1975, **52**, 553
32 A.A. Tsyganenko and V.N. Filmonov, *J. Mol. Struct.*, 1973, **19**, 579
33 F. Boccuzzi, A. Chiorino, M. Manzoli, D. Andreeva and T. Tabakova, *J. Catal.*, 1999, **188**, 176
34 M. Manzoli, A. Chiorino and F. Boccuzzi, *Surf. Sci.*, 2003, **532-535**, 377
35 K. Pokrovski, K.T. Jung and A.T. Bell, *Langmuir*, 2001, **17**, 4297
36 F. Boccuzzi, A. Chiorino, M. Manzoli, P. Lu, T. Akita, S. Ichikawa and M. Haruta, *J. Catal.*, 2001, **202**, 256
37 K.H. Jacob, E. Knözinger and S. Benler, *J. Mater. Chem.*, 1993, **3**, 651
38 H.W. Liu, L.B. Feng, X.S. Zhang and Q.J. Xue, *J. Phys. Chem.*, 1995, **99**, 332
39 K.G. Azzam, I.V. Babich, K. Seshan and L. Lefferts, *J. Catal.*, 2007, **251**, 153
40 H. Sakurai, A.Ueda, T. Kobayashi and M. Haruta. *Chem. Commun.*, 1997, 271
41 S. Carrettin, P. Concepcion, A. Corma, J.M. Lopez Nieto and V.F. Puntes, *Angew. Chem. Int. Ed.*, 2004, **43**, 2538
42 S.H. Overbury, V. Schwartz, D.R. Mullins, W.F. Yan and S. Dai, *J. Catal.*, 2006, **241**, 56
43 N. Lopez, T.V.W. Janssens, B.S. Clausen, Y. Xu, M. Mavrikakis, T. Bligaard and J.K. Nørskov, *J. Catal.*, 2004, **223**, 232
44 X. Zhang, H. Shi and B.-Q. Xu, *Angew. Chem. Int. Ed.*, 2005, **44**, 7132